IIETA International Information and Engineering Technology Association
Advancing the World of Information and Engineering

Journal Européen des Systèmes Automatisés
Vol. 59, No. 3, March, 2026, pp. 815-823
Journal homepage: http://iieta.org/journals/jesa

Artificial Bee Colony and Whale Optimization Algorithm-Tuned Double-Loop PI Control of Charging and Discharging Current in Meca-Electrical Wind Pumping Systems

Abdelkader Elmeddah[1,2*], Djalloul Achour[1,3]

[1] Department of Electronics, Faculty of Technology, Hassiba Benbouali University of Chlef, Hay Salem 02000, Algeria
[2] Laboratory of Electrical Engineering and Renewable Energies, Faculty of Technology, Hassiba Benbouali University of Chlef, Chlef 02000, Algeria
[3] Laboratory of Applied Automation, Boumerdes University, Boumerdes 35000, Algeria

Corresponding Author Email: a.elmeddah@univ-chlef.dz

https://doi.org/10.18280/jesa.590323

Received: 3 January 2026
Revised: 27 February 2026
Accepted: 8 March 2026
Available online: 31 March 2026

Keywords:
double-loop Proportional-Integral controller, Artificial Bee Colony, Whale Optimization Algorithm, bidirectional DC-DC converter, battery bank

ABSTRACT

The Meca-Electrical Wind Pumping System (MEWPS) offers a sustainable solution for providing water in rural and off-grid regions, thanks to its integrated design that combines mechanical and electrical wind pumping systems. Previous studies primarily focused on power conversion and did not provide a realistic dynamic representation of the system. In this work, a comprehensive dynamic model of MEWPS was developed, including the separately excited DC machine, bidirectional DC-DC converter, and battery bank. A double-loop Proportional-Integral (PI) control strategy was implemented to regulate the battery charging and discharging currents precisely. The PI gains were optimized using Artificial Bee Colony (ABC) and Whale Optimization Algorithm (WOA). A comprehensive evaluation was carried out through cost function convergence, PI parameter convergence, and performance indices such as IAE, ISE, ITAE, overshoot, steady-state error, and settling time. Dynamic performance was further examined under varying load torque, along with the analysis of DC machine speed, armature voltage, charging/discharging currents, and battery state-of-charge (SOC). The results clearly demonstrate the mode-dependent superiority of the optimization algorithms under charging and discharging conditions and emphasize the critical role of coordinated multi-loop PI tuning in achieving robust and energy-efficient operation of MEWPS.

1. INTRODUCTION

The increasing global demand for sustainable energy solutions has accelerated the integration of renewable technologies into water pumping applications, particularly in remote and rural regions where access to conventional power grids is limited [1, 2]. Among these technologies, Meca-Electrical Wind Pumping Systems (MEWPS) have gained increasing attention because they introduce a new concept of wind-pumping technology and combine the strengths of both mechanical and electrical wind pumping systems to achieve greater reliability and environmental sustainability [3]. However, the performance of MEWPS is strongly dependent on effective energy management and the stable delivery of power to storage units.

One of the key challenges is the regulation of charging and discharging currents, since improper current control can shorten battery lifetime, increase energy losses, and degrade overall system efficiency [4, 5]. To address this, advanced control strategies are needed to ensure accurate current tracking under dynamic operating conditions. The bidirectional DC-DC converter plays a central role in this framework by adjusting voltage levels and managing the bidirectional flow of energy between the DC machine and the battery bank.

Although conventional Proportional-Integral (PI) controllers are widely used in renewable energy systems for their simplicity and ease of implementation, their performance is highly dependent on parameter tuning, particularly in the presence of nonlinearities and varying load conditions [6]. To overcome these limitations, bio-inspired optimization techniques such as Artificial Bee Colony (ABC) and Whale Optimization Algorithm (WOA) have been employed to enhance controller efficiency and robustness.

In this paper, a double-loop PI-based control approach for MEWPS is proposed, where the PI parameters are tuned using ABC and WOA algorithms. The contributions of this work are:

- The design of an efficient double-loop PI current control strategy for battery charging and discharging regulation.
- The application of ABC and WOA to optimize PI gains for improved stability and reduced energy consumption.
- A comprehensive comparative evaluation covering convergence characteristics, classical performance indices (IAE, ISE, ITAE), dynamic behavior under load torque variations, and battery state-of-charge (SOC)

analysis.

2. ELECTRICAL PART MODEL OF MEWPS

As depicted in Figure 1. The MEWPS is designed to harness wind energy and transform it into both mechanical and electrical power for water pumping applications. It consists of several interconnected subsystems including a wind turbine, gearbox, DC machine, bidirectional DC-DC converter, battery storage, and pump cylinder that operate in coordination to ensure stable and efficient performance [7].

The bidirectional DC-DC converter plays a key role in regulating power flow by storing surplus energy in the battery during periods of high wind and supplying it back when wind power is insufficient [8]. The DC machine functions as the main electromechanical converter, with its speed directly influencing both charging and discharging of battery bank, highlighting the need for precise control. These components represent the core of the proposed model, with reliable and stable control of the bidirectional DC-DC converter established as the primary objective. The modeling will focus on the electrical part because current control is achieved through the bidirectional DC-DC converter control.

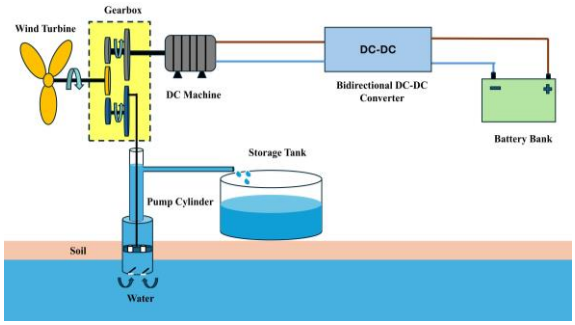

Figure 1. Meca-Electrical Wind Pumping System (MEWPS)

2.1 Bidirectional DC-DC converter model

The bidirectional DC-DC converter serves as the main energy management unit, enabling both charging and discharging of the battery [9]. By adjusting its duty cycle, the system not only determines the direction of energy transfer but also controls the magnitude of the power flow, thereby ensuring efficient utilization of wind energy and stable operation under variable wind conditions [10].

2.1.1 Charging mode

In this mode, the bidirectional DC-DC converter functions as a buck converter [11]. As a result, excess energy is transformed from the DC machine to the battery. The duty cycle regulates the output voltage, enabling efficient charging and protecting the battery from overvoltage. The output voltage is determined as follows:

$$V_{battery} = D.V_{DC\ machine} \tag{1}$$

where, $V_{battery}$ is battery voltage (V), $V_{DC\ machine}$ is DC machine voltage (V), D is duty cycle.

2.1.2 Discharging mode

When wind power is insufficient, the converter operates in boost mode, drawing energy from the battery to supply the DC machine. The duty cycle ensures stable voltage delivery, maintaining machine performance while avoiding deep discharge. The output voltage determined as follow:

$$V_{DC\ machine} = \frac{D}{1-D}\, V_{battery} \tag{2}$$

The determined parameters of bidirectional DC-DC converter are displayed in Table 1.

Table 1. Parameters of bidirectional DC-DC converter

Parameters	Values
Switching frequency ($\mathbf{S_f}$)	10 (KHz)
Duty cycle (**D**)	0 to 0.95
Inductor (**L**)	1.23×10^{-3} (H)
Capacitor (**C**)	0.002565 (F)
Bus Capacitor ($\mathbf{C_{bus}}$)	0.001 (F)

2.2 DC machine model

The dynamic behavior of the separately excited DC machine is modeled through its electrical and mechanical subsystems [12]. The armature voltage equation accounts for resistance, inductance, and back EMF, while the back EMF is proportional to speed. The electromagnetic torque depends on the armature current, and the mechanical equation relates torque balance to rotor acceleration, inertia, and viscous friction [13]. Together, these equations describe the coupling between electrical input, torque production, and speed response under varying load conditions [14]. This DC machine can be described using these dynamic equations:

- Armature voltage equation

$$V_a = R_a.i_a(t) + L_a.\frac{di_a(t)}{dt} + e_b(t) \tag{3}$$

where, V_a is armature voltage (V), R_a is armature resistor (Ω), i_a is armature current (A), L_a is armature inductance (H), e_b is back emf force (V).

- Back EMF relation

$$e_b = K_e.\omega = K_{af}.I_f \tag{4}$$

where, K_e is voltage constant, ω is DC machine speed (rad/s), K_{af} is field-armature mutual inductance (H), I_f is field current (A).

- Electromagnetic torque equation

$$T_e = K_t.i_a \tag{5}$$

where, K_t is torque constant.

- Mechanical dynamic equation of DC machine

$$J\frac{d\omega}{dt} = T_e - T_L - B_m.\omega - T_f \tag{6}$$

where, T_e is electrical torque (N.m), T_L is load torque (N.m), J is inertia $(Kg.m^2)$, B_m is viscous friction coefficient (N.m.s), T_f is coulomb friction torque (N.m).

The parameters of the separately excited DC machine are identified and presented in Table 2.

Table 2. DC machine parameters

Parameters	Values
Armature voltage	240 V
Armature resistance	2.581 Ω
Field voltage	300 V
Field resistance	281.3 Ω
Field armature mutual inductance	0.9483

2.3 Battery bank model

The battery in MEWPS acts as an energy buffer, storing excess energy during high wind and supplying it during low wind conditions. Its behavior is commonly represented by a simplified dynamic model that relates the SOC to charging and discharging currents, while the terminal voltage is influenced by open-circuit voltage, internal resistance, and polarization effects [15]. This model effectively captures the essential dynamics for system-level analysis and controller design. its behavior can be represented by a simplified dynamic model, expressed as:

$$V_{battery}(t) = V_{oc} - R_{int} \cdot i_{battery}(t) \quad (7)$$

$$SOC(t) = SOC(0) - \frac{1}{C_{battery}} \int i_{battery}(t)\, dt \quad (8)$$

where, V_{oc} is open-circuit voltage (V), R_{int} is internal resistance (Ω), $i_{battery}$ is charging/discharging current, and SOC is state of charge with capacity $C_{battery}$.

The battery parameters are determined in Table 3.

Table 3. Battery bank parameters

Parameters	Values
Maximum Capacity	200 Ah
Cut-off voltage	90 V
Fully charged voltage	139.6785 V
Nominal discharge current	86.9585 A
Inter resistance	0.006 Ω
Capacity at nominal voltage	180.8696 Ah

3. CONTROL STRATEGY

The double-loop PI controller works with two connected loops that share the task of keeping the system stable [16]. In the outer loop, the PI controller compares the target armature voltage resulting from the required DC machine speed and load torque with the actual DC machine voltage and then produces a current reference for the inner loop. The inner loop reacts quickly, making sure the battery's current follows that reference closely, which helps the system handle disturbances right away. By working together, these two loops allow the battery to maintain its current smoothly, even when the load or speed keeps changing, as shown in Figure 2.

3.1 Optimization methods (ABC and WOA)

Effective operation of the double-loop PI controller requires proper tuning of proportional and integral gains. Traditional approaches such as the Cohen-Coon method, trial-and-error tuning, or root locus often these methods can't get the right gains for control complex and nonlinear systems like MEWPS. In contrast, optimization techniques can automatically determine optimal gain values, leading to improved performance and reduced errors.

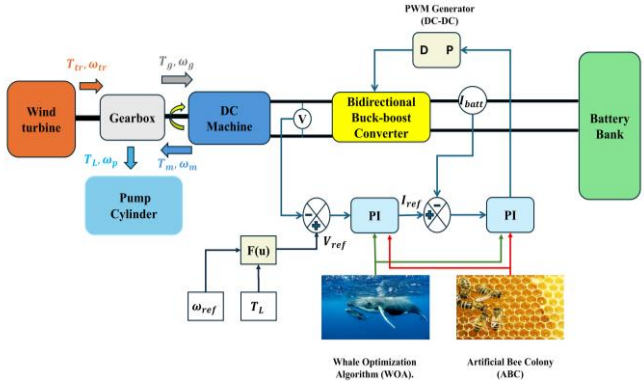

Figure 2. Structure of the double-loop Proportional-Integral (PI) controller for control the Meca-Electrical Wind Pumping System (MEWPS)

3.1.1 Artificial Bee Colony algorithm

The Artificial Bee Colony algorithm models the foraging behavior of honey bees in search of nectar sources [17]. In the context of PI controller tuning, each food source represents a potential solution set of parameters $(K_{P1}, K_{I1}, K_{P2}, K_{I2})$[18]. The collective intelligence of bees enables efficient exploration and exploitation of the search space.

3.1.2 Whale Optimization Algorithm

The Whale Optimization Algorithm is inspired by the bubble-net hunting strategy of humpback whales, where they cooperate to trap prey in spirals [19]. For controller tuning, each whale represents a candidate solution $(K_{P1}, K_{I1}, K_{P2}, K_{I2})$, and the population collectively searches for the best gains [20].

ABC and WOA were independently applied to tune the double-loop PI controller in MEWPS due to their individual strengths. ABC provides robust exploration of the solution space, reducing the risk of premature convergence to suboptimal gains, while WOA achieves fast and efficient convergence toward optimal parameters.

3.2 Optimization configuration for double-loop Proportional-Integral

The optimization configuration defines the framework for tuning the double-loop PI controllers, specifying the decision variables, objective function, constraints, and operational flowchart under which the ABC and WOA algorithms are executed.

3.2.1 Decision variables

The PI parameters in the double-loop structure include the proportional and integral gains for both the current loop (K_{P1}, K_{I1}) and the voltage loop (K_{P2}, K_{I2}). These parameters are carefully selected to ensure system stability while allowing sufficient flexibility for performance tuning.

3.2.2 Objective function

The double-loop PI controller in the MEWPS is tuned by minimizing a cost function J that quantifies the system's performance. The PI parameters $(K_{P1}, K_{I1}, K_{P2}, K_{I2})$ are applied to the Simulink model, and the resulting voltage,

current, and speed responses are compared to their reference signals. The cost function is defined as a weighted integral of absolute errors (IAE):

$$J = \alpha \int_0^T |e_V(t)|\, dt + \beta \int_0^T |e_I(t)|\, dt + \gamma \int_0^T |e_S(t)|\, dt \qquad (9)$$

where, e_V, e_I, and e_S are the voltage, current, and speed errors, and α, β, γ are weighting factors.

Minimizing Jensures improved transient response, reduced steady-state error, and enhanced robustness under the nonlinear and time-varying dynamics of MEWPS.

3.2.3 Constraints

Practical limits are set on the PI gains to ensure stability and define the feasible search space for the ABC and WOA optimization algorithms, allowing them to identify optimal and physically meaningful controller parameters. The tuning ranges for PI parameters are defined as follows:

$$\begin{aligned} 0 \le K_{P1} \le 10 \\ 0 \le K_{I1} \le 50 \\ 0 \le K_{P2} \le 50 \\ 0 \le K_{I2} \le 50 \end{aligned} \qquad (10)$$

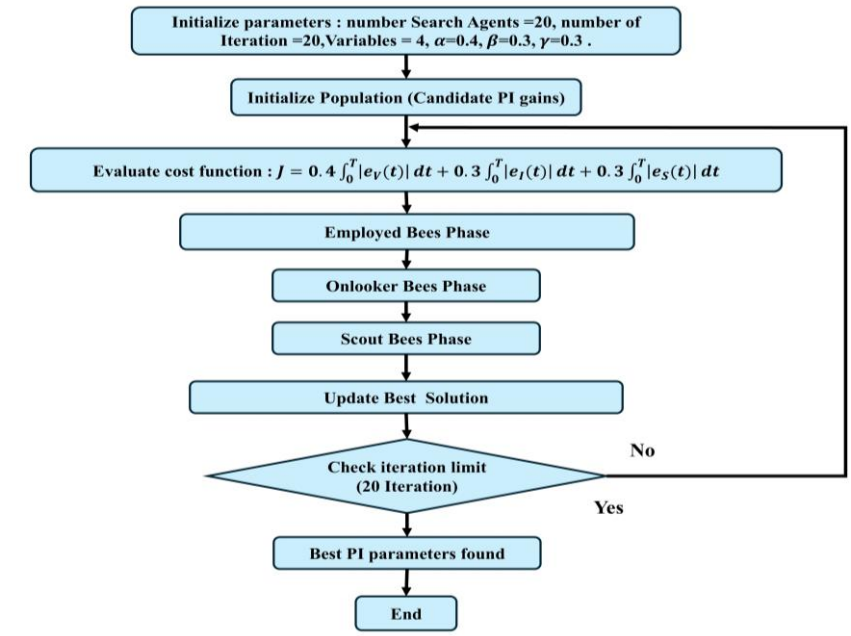

Figure 3. Artificial Bee Colony (ABC) flowchart

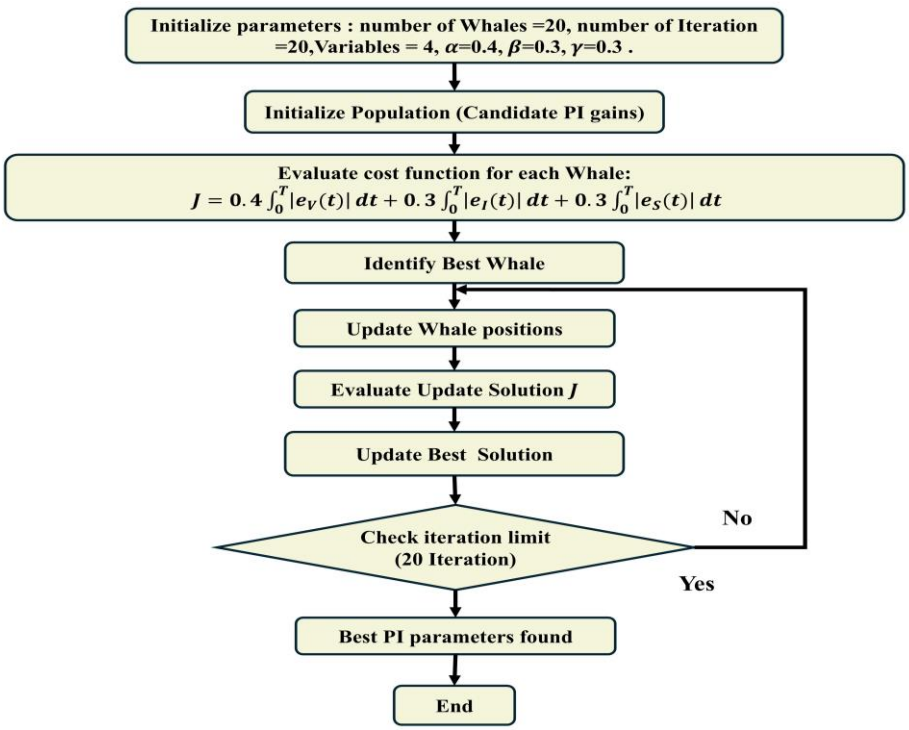

Figure 4. Whale Optimization Algorithm (WOA) flowchart

3.2.4 Flowcharts

Figures 3 and 4 show the flowcharts of the ABC and WOA algorithms, respectively, highlighting the sequential steps and differences in their optimization procedures. For a fair and unbiased comparison between the ABC and WOA optimization algorithms, both methods were implemented using identical parameter settings. The population size was fixed at 20 individuals, and the maximum number of iterations was set to 20, and the stopping criterion was defined as a maximum of 20 iterations for both algorithms. The optimization process involved four decision variables corresponding to the PI controller parameters. In addition, the same objective function with weighting factors $\alpha = 0.4$, $\beta = 0.3$, and $\gamma = 0.3$ was used. These parameter values were chosen to ensure sufficient exploration and exploitation capabilities while maintaining a reasonable computational cost, which is suitable for control-oriented optimization problems.

4. RESULTS AND DISCUSSION

This section showcases the results of tuning the double-loop PI controller using the ABC and WOA algorithms, with the discussion concentrating on three key point:

- Cost Function and PI Parameter Convergence.
- Performance Indices (IAE, ISE, ITAE, Overshoot, Steady-State Error).
- Dynamic Analysis: DC Machine Speed, Armature Voltage, Charging/Discharging Current, SOC of battery bank.

4.1 Cost function and Proportional-Integral parameter convergence

Figure 5 illustrated the convergence patterns of the four PI controller parameters ($K_{P1}, K_{I1}, K_{P2}, K_{I2}$) over 20 iterations for the two optimization methods: ABC and WOA. In the WOA subplot (top), the convergence of K_{P2} and K_{I2} was somewhat irregular, exhibiting significant fluctuations between iterations 10 and 14 before stabilizing and maintaining consistent values until the 20th iteration. This behavior indicated that WOA focused on exploiting promising solutions while restricting extensive exploration of the search space. Meanwhile, K_{P1} and K_{I1} underwent slight adjustments during the initial iterations before reaching steady-state values. Overall, this demonstrated WOA's ability to balance exploration and exploitation, enabling efficient convergence to high-quality parameter sets.

In contrast, the ABC subplot (bottom) began with constant parameter values and stable behavior up to iteration 11. At this point, K_{P2} increased sharply from 8 to 50, then gradually decreased over the next five iterations, settling near 43 by the end. Meanwhile, K_{I2}dropped steadily from iteration 11 until reaching 0, before rising again to around 9 after iteration 18. K_{I1} remained stable until iteration 11, where it underwent a slight adjustment, while K_{P1} stayed nearly constant throughout all iterations. This pattern showed that ABC introduced sudden changes in parameter values after the initial stable phase, particularly for K_{P2} and K_{I2}. Such behavior reflected a tendency toward unstable exploration with limited exploitation of promising solutions, which prevented premature convergence but resulted in slower and less predictable optimization performance. Overall, the results highlighted that WOA achieved faster and more stable parameter convergence, making it better suited for precise and reliable PI controller tuning. In contrast, ABC's abrupt and inconsistent parameter adjustments indicated stronger exploration but less effective exploitation, leading to slower and less predictable performance.

The convergence performance of the cost function, illustrated in Figure 6, showed notable differences between the WOA and the ABC algorithm. WOA exhibited a steep reduction in the cost function during the initial iterations, reaching a value of approximately 10.5 by the eleventh iteration, after which no further significant improvement was observed. Conversely, ABC showed limited progress during the first eleven iterations but achieved a gradual reduction thereafter, ultimately converging to a lower final cost than WOA. This behavior emphasized the trade-off between the rapid early convergence of WOA and the enhanced long-term accuracy of ABC.

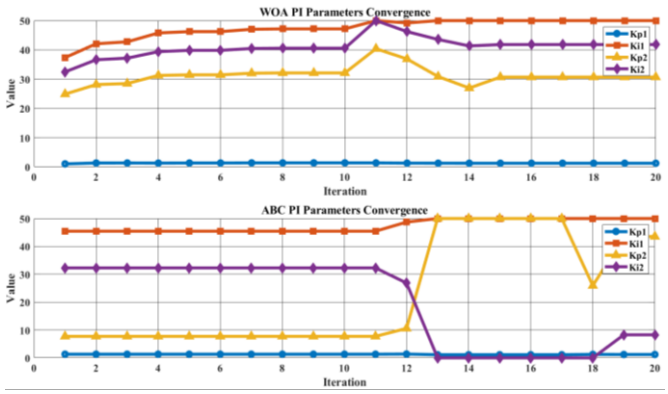

Figure 5. Proportional-Integral (PI) parameters convergence

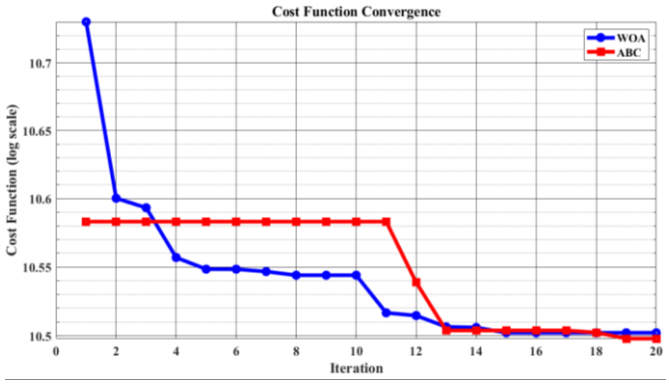

Figure 6. Cost function convergence

4.2 Performance indices

The comparative performance results of the double-loop PI controller optimized using WOA and ABC were summarized in Table 4. Both optimization methods delivered satisfactory dynamic and steady-state responses, but with some distinct differences. ABC achieved lower error indices, with an IAE of 8.6413, an ISE of 713.07, and an ITAE of 0.45193, demonstrating its effectiveness in minimizing cumulative and squared error metrics. This suggested that ABC provided stronger robustness and improved transient behavior by reducing overall error magnitudes. In contrast, WOA offered a slight advantage in overshoot suppression, with a maximum overshoot of 2.7705 compared to ABC's 2.7742, which, although numerically close, reflected its ability to better

regulate the peak response. Despite these differences, both controllers converged to the same steady-state value of 130 and achieved an identical settling time of 1 s, confirming their capability to ensure stability. Overall, ABC demonstrated superior transient response and error reduction, making it advantageous for applications that prioritized precision and robustness, while WOA proved beneficial in scenarios where overshoot minimization was critical.

Table 4. The comparative performance results

Algorithm	K_{P1}	K_{I1}	K_{P2}	K_{I2}	IAE	ISE	ITAE	Overshoot	SteadyState	Settling Time
WOA	1.2372	50	30.681	41.803	8.6554	713.77	0.4534	2.7705	130	1
ABC	1.2051	50	43.535	8.272	8.6413	713.07	0.45193	2.7742	130	1

4.3 Dynamic analysis

The variation of charging and discharging current in the MEWPS depends on changes in the DC machine speed as well as the load torque. In this scenario, the speed is considered constant while the load is varied to examine the system behavior and observe how the charging/discharging current, DC machine voltage, and battery SOC change. Proper control of the machine voltage (Outer loop) and charging/discharging current (Inner loop) ensures effective regulation of the machine speed despite variations in the load.

The load torque applied to the DC machine is examined under two operating modes. In motor mode, the machine operates at a reference speed of 150 rad/s, while the load torque is varied stepwise from 10 N.m (0-10 s) to 13 N.m (10-17.5 s), and then reduced to 8 N.m (17.5–27.5 s). Subsequently, the machine operates in generator mode with a reference speed of 170 rad/s, where negative load torque values of -12 N.m (27.5–35.6 s), -10 N.m (35.6–42 s), and -14 N.m (42–50 s) are applied. The corresponding load torque profiles for both operating modes are depicted in Figure 7.

Figure 8 illustrated the dynamic response of the DC machine under varying load conditions and revealed the intricate interaction between the PI gains of the inner and outer loops. In motor mode, the ABC algorithm, with an inner-loop proportional gain (K_{P1} = 1.2051) and outer-loop proportional gain (K_{P2} = 43.535), exhibited rapid and stable tracking of the reference speed (150 rad/s). The relatively lower K_{P1} reduced the current ripple, while the higher K_{P2} allowed the system to respond effectively to load variations (10, 13, and 8 N.m), ensuring minimal overshoot and smooth transient performance. In contrast, the WOA algorithm, with (K_{P1} = 1.2372) and (K_{P2} = 30.681), generated a faster initial current response due to the higher K_{P1}, but this came at the cost of increased current and voltage ripple, resulting in higher overshoot. The higher outer-loop integral gain (K_{I2} = 41.803) in WOA helped eliminate steady-state speed error quickly, but slightly amplified transient oscillations during sudden load changes.

During generator mode, the WOA algorithm demonstrated its advantage due to the high K_{I2}, which ensured smoother voltage and current profiles (-12, -10, and -14 N.m) and reduced ripple in the DC machine voltage (140-150 V), thereby protecting the battery. ABC, while maintaining faster speed tracking, produced slightly higher current and voltage ripple during charging due to its lower (K_{I2} = 8.272), highlighting the mode-dependent performance superiority of each algorithm. The analysis showed that inner-loop gains primarily affected the speed and current ripple, while outer-loop gains governed the tracking accuracy and steady-state performance of speed, emphasizing the importance of coordinated tuning.

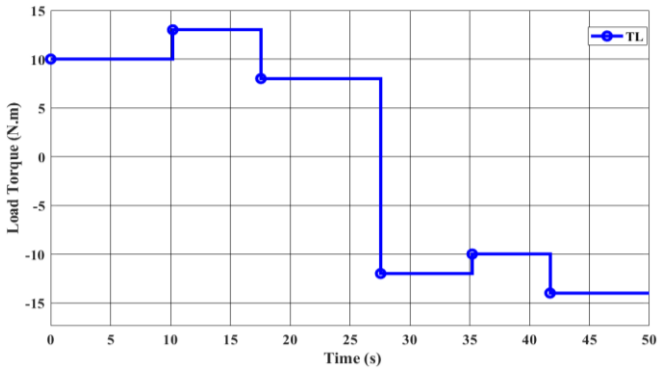

Figure 7. Load torque

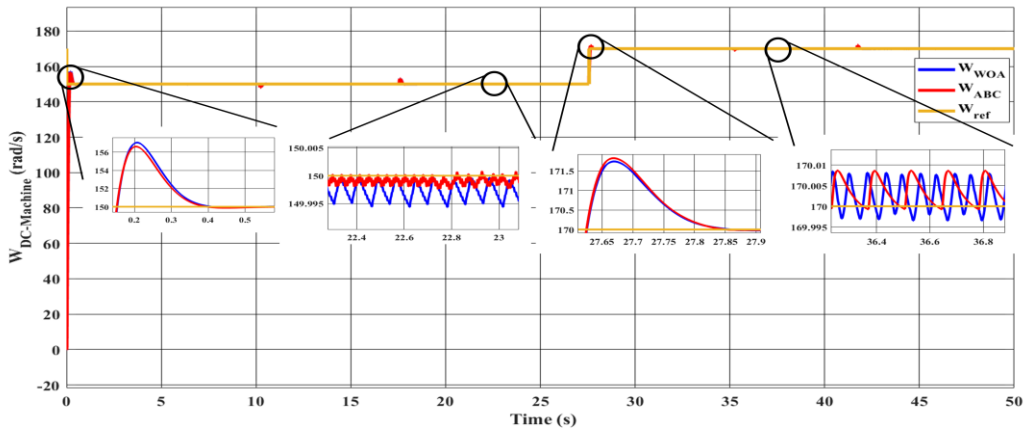

Figure 8. Dynamic speed response of DC machine

Figure 9 showed that the DC machine voltage behavior was similarly influenced by the PI gains. In motor mode (Discharging mode), ABC achieved more stable voltage profiles (174.51-187.4 V) due to its lower (K_{P1} = 1.2051),

which reduced ripple during load transitions. WOA, with a higher (K_{P1} = 1.2372), exhibited increased voltage fluctuations during motor mode, although its higher (K_{I2} = 41.803) mitigated steady-state errors over time. During generator mode (charging mode), WOA maintained a smoother voltage (138.9-149 V) thanks to the high K_{I2}, which suppressed ripple and provided better battery protection during charging. ABC, while slightly faster in speed tracking, resulted in higher voltage fluctuations. This confirmed that the inner-loop proportional gain primarily affected ripple magnitude, whereas the outer-loop integral gain governed voltage stability and long-term tracking, linking voltage dynamics to overall system performance.

The PI gains directly influenced the dynamic behavior of the battery currents, as depicted in Figure 10. In discharging mode, ABC's lower (K_{P1} = 1.2051) reduced the current ripple, resulting in smoother discharge currents (16.25, 22, and 12.6 A) and improved SOC management. WOA, with a slightly higher (K_{P1} = 1.2372), produced faster transient current responses but suffered from more pronounced ripple, which could accelerate SOC depletion under high-load conditions. During charging mode, WOA's higher (K_{I2} = 41.803) ensured that the charging currents (-11.5, -9.5, and -12.8A) remained stable despite load variations, thereby contributing to battery protection and reducing energy losses. ABC, with a lower (K_{I2} = 8.272), allowed faster speed tracking but introduced moderate ripple in the charging currents. These observations underscored the interplay between the inner-loop proportional gain and the outer-loop integral gain in determining both transient and steady-state current behavior.

The SOC evolution depicted in Figure 11 reflects the combined effects of PI gain tuning, battery current dynamics, and voltage stability. Smoother discharge currents, achieved through appropriate inner-loop PI gains, reduce current ripple and the associated resistive losses within the battery, leading to a more gradual SOC decrease. In discharging mode, ABC's lower inner-loop proportional gain (K_{P1} = 1.2051) combined with a higher outer-loop proportional gain (K_{P2} = 43.535) resulted in smoother current profiles and a gradual SOC decline from 44.995% to 44.936%, thereby minimizing energy losses and improving efficiency. In contrast, WOA's slightly higher (K_{P1} = 1.2372) produced faster current responses but increased ripple, which amplified instantaneous power losses and caused a slightly faster SOC depletion under fluctuating load conditions. During charging mode, the higher outer-loop integral gain of WOA (K_{I2} = 41.803) ensured well-regulated charging currents and reduced voltage ripple, yielding a controlled SOC increase and enhanced battery protection. Although ABC exhibited slightly higher ripple during charging due to a lower K_{I2}, it provided faster speed tracking. Overall, these results highlight the critical role of coordinated tuning of all four PI gains (K_{P1} , K_{I1} , K_{P2} , and K_{I2}) in optimizing SOC behavior while balancing speed tracking performance and ripple suppression, thus ensuring stable and efficient battery operation.

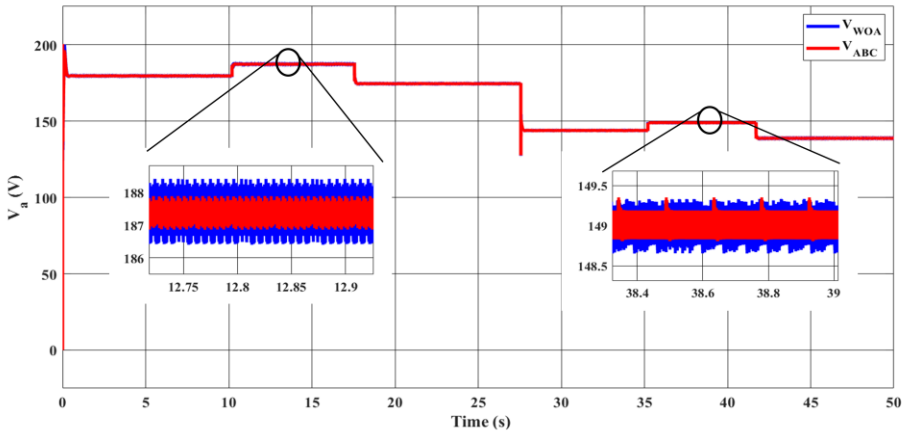

Figure 9. The dynamic voltage of DC machine

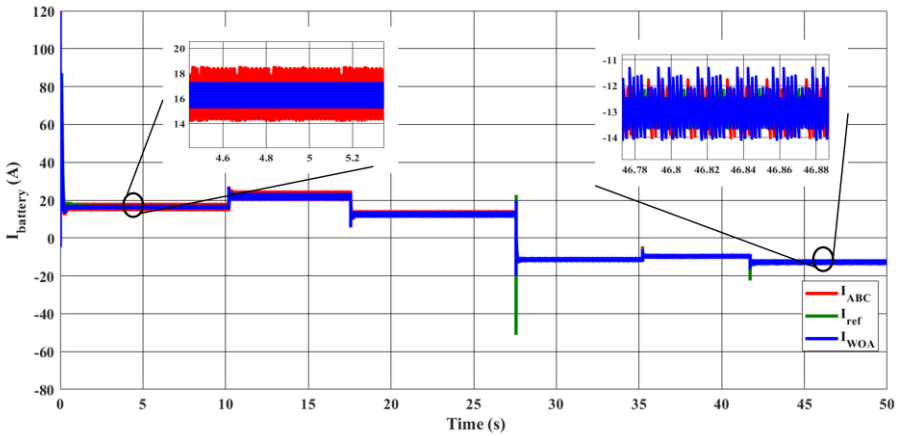

Figure 10. Charging and discharging of battery current

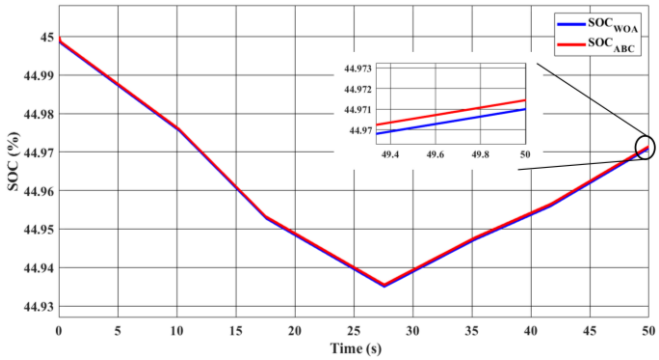

Figure 11. State-of-charge (SOC) of battery

5. CONCLUSION

This work presented an optimized double-loop PI control strategy for MEWPS integrated with a bidirectional DC-DC converter. The inner loop ensures precise current tracking, while the outer loop generates the reference current to maintain desired DC machine speed. The coordinated tuning of PI parameters is critical in achieving fast speed response, low ripple, voltage stability, and efficient battery SOC management. By employing ABC and WOA optimization algorithms, the PI gains were effectively tuned to achieve improved stability, accuracy, and robustness. The simulation results revealed a clear mode-dependent performance of the optimization algorithms. In discharging mode, the ABC-based controller achieved smoother current profiles, lower voltage ripple, faster speed tracking, and more efficient state-of-charge utilization. In contrast, during charging mode, the WOA-based controller ensured smoother voltage and current responses, thereby enhancing battery protection and overall charging stability. These findings clarify the interaction between inner and outer PI gains and system dynamics, guiding energy-efficient and robust MEWPS design.

The study contributes theoretically by establishing the first detailed dynamic model of MEWPS, linking inner- and outer-loop PI gains to DC machine voltage, charging/discharging current dynamics, speed tracking, and battery SOC. The revealed complementary behavior of ABC and WOA offers insights into trade-offs between dynamic response, ripple suppression, and energy efficiency, providing practical tuning guidelines. Overall, the proposed control strategy enhances robustness, energy efficiency, and practical applicability of MEWPS, with future work aiming to integrate advanced control techniques such as MPC, FLC, and ANN-based controllers to improve adaptability and overall system performance.

ACKNOWLEDGMENT

This research was supported by the Algerian Ministry of Higher Education and Scientific Research.

REFERENCES

[1] Khalil, M., Sheikh, S.A. (2024). Advancing green energy integration in power systems for enhanced sustainability: A review. IEEE Access, 12: 151669-151692. https://doi.org/10.1109/ACCESS.2024.3472843

[2] Zabihi, A., Pidikiti, T., Varanasi, L.N.S., Kalnoor, G., Akkurt, I., Murali Krishna, V.B. (2025). Solar-powered pumping for alleviating energy poverty: Sustainable solutions for agriculture sector in Portugal. IEEE Access, 13: 105077-105090. https://doi.org/10.1109/ACCESS.2025.3579783

[3] Djalloul, A., Mohamed, K. (2023). Improvement of the Meca-electrical wind pumping system. In 2023 14th International Renewable Energy Congress (IREC), Sousse, Tunisia, pp. 1-6. https://doi.org/10.1109/IREC59750.2023.10389467

[4] Prakash, K., Ali, M., Siddique, M.N.I., Chand, A.A., Kumar, N.M., Dong, D., Pota, H.R. (2022). A review of battery energy storage systems for ancillary services in distribution grids: Current status, challenges and future directions. Frontiers in Energy Research, 10: 971704. https://doi.org/10.3389/fenrg.2022.971704

[5] Yahmadi, R., Brik, K., ben Ammar, F. (2023). Reducing the impact of degradation causes on electrical power sources in the photovoltaic water pumping system. Renewable Energy Focus, 47: 100509. https://doi.org/10.1016/j.ref.2023.100509

[6] Warrier, P., Shah, P. (2021). Fractional order control of power electronic converters in industrial drives and renewable energy systems: A review. IEEE Access, 9: 58982-59009. https://doi.org/10.1109/ACCESS.2021.3073033

[7] Djalloul, A., Mohamed, K. (2020). New concept of wind pumping system: Introduction and state of the art. In 2020 11th International Renewable Energy Congress (IREC), Hammamet, Tunisia, pp. 1-5. https://doi.org/10.1109/IREC48820.2020.9310383

[8] Mandal, S., Prabhakaran, P. (2025). A high-efficiency, high-gain, non-isolated bidirectional DC-DC converter for interfacing DC grid-connected energy storage systems. IEEE Transactions on Consumer Electronics, 72(1): 134-146. https://doi.org/10.1109/TCE.2025.3648303

[9] Eroğlu, F., Kurtoğlu, M., Vural, A.M. (2021). Bidirectional dc–dc converter based multilevel battery storage systems for electric vehicle and large-scale grid applications: A critical review considering different topologies, state-of-charge balancing and future trends. IET Renewable Power Generation, 15(5): 915-938. https://doi.org/10.1049/rpg2.12042

[10] Zeng, J.W., Du, X., Yang, Z.X. (2021). A multiport bidirectional DC–DC converter for hybrid renewable energy system integration. IEEE Transactions on Power Electronics, 36(11): 12281-12291. https://doi.org/10.1109/TPEL.2021.3082427

[11] Sreejyothi, K.R., Balakrishnakothapalli, Chenchireddy, K., Sydu, S.A., Kumar, V., Sultana, W. (2022). Bidirectional battery charger circuit using buck/boost converter. In 2022 6th International Conference on Electronics, Communication and Aerospace Technology, Coimbatore, India, pp. 63-68. https://doi.org/10.1109/ICECA55336.2022.10009062

[12] Acevedo, D.M., Parraguez-Garrido, I., Gil-González, W., Montoya, O.D., González-Castaño, C. (2025). Adaptive passivity-based control for dc motor speed regulation in DC-DC converter-fed systems. IEEE Access, 13: 131957-131966. https://doi.org/10.1109/ACCESS.2025.3592594

[13] Abouseda, A.I., Doruk, R., Emin, A., Akdeniz, O.

(2025). Modeling, dynamic characterization, and performance analysis of a 2.2 kW BLDC motor under fixed load torque levels and variable speed inputs: An experimental study. Actuators, 14(8): 400. https://doi.org/10.3390/act14080400

[14] Patel, D., Shah, S., Chothani, N., Raichura, M. (2021). Dynamic psychoanalysis of DC separately excited machine on laboratory visualization. In 2021 International Conference on Sustainable Energy and Future Electric Transportation (SEFET), Hyderabad, India, pp. 1-6. https://doi.org/10.1109/SeFet48154.2021.9375770

[15] Pavković, D., Cipek, M., Kvaternik, K., Faiz, N., Shambilova, A. (2025). Enhancing lithium titanate battery charging: Investigating the benefits of open-circuit voltage feedback. Energies, 18(15): 3946. https://doi.org/10.3390/en18153946

[16] Yanarates, C., Zhou, Z.F. (2022). Design and cascade PI controller-based robust model reference adaptive control of DC-DC boost converter. IEEE Access, 10: 44909-44922. https://doi.org/10.1109/ACCESS.2022.3169591

[17] Wang, Y.C., Jiao, J., Liu, J.H., Xiao, R.B. (2022). A labor division artificial bee colony algorithm based on behavioral development. Information Sciences, 606: 152-172. https://doi.org/10.1016/j.ins.2022.05.065

[18] Raizada, V., Singh, N.J., Chopra, V., Kaur, J., Lamba, R. (2026). Fractional order PID controller design using predator effect inspired artificial bee colony algorithm. Journal of Engineering Research. https://doi.org/10.1016/j.jer.2026.02.020

[19] Abualigah, L., Abualigah, R., Ikotun, A.M., Zitar, R.A., Alsoud, A.R., Khodadadi, N., Ezugwu, A.E., Hanandeh, E.S., Jia, H.M. (2024). Whale optimization algorithm: Analysis and full survey. In Metaheuristic Optimization Algorithms, pp. 105-115. https://doi.org/10.1016/B978-0-443-13925-3.00015-7

[20] Mahapatro, S.R., Khadanga, R.K. (2026). Optimal decentralized PI control design for a benchmark process control system with time delay: A modified whale optimization algorithm. Franklin Open, 15: 100534. https://doi.org/10.1016/j.fraope.2026.100534